Carbon 152 (2019) 865–872

Contents lists available at ScienceDirect

Carbon

journal homepage: www.elsevier.com/locate/carbon

Terahertz dielectric anisotropy enhancement in dual-frequency liquid crystal induced by carbon nanotubes

Yun-Yun Ji [a], Fei Fan [a, c, *], Shi-Tong Xu [a], Jian-Ping Yu [a], Yan Liu [a], Xiang-Hui Wang [a], Sheng-Jiang Chang [a, b, **]

[a] Institute of Modern Optics, Nankai University, Tianjin, 300350, China
[b] Tianjin Key Laboratory of Optoelectronic Sensor and Sensing Network Technology, Tianjin, 300350, China
[c] State Key Laboratory of Applied Optics, Changchun Institute of Optics, Fine Mechanics and Physics, Chinese Academy of Sciences, Changchun, 130033, China

ARTICLE INFO

Article history:
Received 24 April 2019
Received in revised form
12 June 2019
Accepted 26 June 2019
Available online 27 June 2019

Keywords:
Terahertz
Dual-frequency liquid crystals
Carbon nanotube
Phase devices

ABSTRACT

Dual-frequency liquid crystals (DFLCs), the mixture of positive and negative liquid crystal (LC) molecules, exhibit unique alternating (*AC*) frequency dependent anisotropic properties. Carbon nanotube (CNT), as a novel nanomaterial with strong anisotropy, has attracted much attention in recent years. Herein, we investigate the tunable terahertz birefringence and phase shift characteristics of the DFLC doped with CNT (CNT-LC) by using the terahertz time-domain polarization spectroscopy. The results show that the CNT-LC (1.5 wt%) can reach 0.5π at 0.793 THz, which can be used as a tunable THz phase shifter that is 0.12π higher than the pure DFLCs. Furthermore, through measuring the output polarization state, it is confirmed that the dielectric anisotropy enhancement mechanism of CNT-LC originates from the surface interaction between CNTs and LC molecules. Therefore, a tunable quarter-wave plate with the active polarization conversion from linearly polarized (LP) to LP or LP to circularly polarized (CP) can be realized at 0.925 THz in the CNT-LC, while the pure DFLC cannot be achieved at the same frequency. The dielectric anisotropy enhancement of CNT-LC shows its utility in the improvement of various tunable terahertz LC phase shifter and wave plate.

1. Introduction

Terahertz (THz, from 0.1–10 × 10^{12} Hz) waves have the superiority of low photon energy, high penetrability and fingerprint spectrum, which can offer great potential for application in security screening, nondestructive detection, material spectroscopy and wireless communication [1–4]. Benefit from the rapid development of THz sources [5,6] and detectors [7,8], THz functional devices are highly in demand to guide and modulate THz waves in an efficient way, such as waveguides [9], switches [10], filters [11], isolators [12], modulator [13], polarizers [14] and phase shifters [15]. Phase and polarization, as the basic parameters of electromagnetic wave, not only carry valuable information but also manipulate the propagation state of THz waves. Therefore, high-performance THz phase and polarization devices are urgently needed for further development of THz technology and its application system [16,17].

Over the past decade, liquid crystals (LCs) have attracted wide attention in the development of tunable phase and polarization control devices thanks to their large optical anisotropy, which can be flexibly controlled by thermal, optical, electrical or magnetic field [18–21]. The optical properties of LCs in the THz regime have been extensively studied in recent years. Vieweg et al. reported the nematic mixture BL037 with a high birefringence of about 0.20 in the frequency range of 0.3–2.5 THz [22]. Pan et al. investigated the ordinary and extraordinary indices of 5CB are $n_o = 1.58$ and $n_e = 1.77$, respectively, giving rise to a birefringence of $\Delta n = n_e - n_o = 0.20 \pm 0.02$ from 0.2 to 1.0 THz [23]. Recently, Wang et al. proposed a new LC mixture NJU-LDn-4 with a large birefringence 0.306 in a broad range from 0.4 to 1.6 THz [24]. Reuter et al. presented two high birefringence LC mixtures with $\Delta n = 0.32$ and $\Delta n = 0.38$ in the frequency range between 0.2 and 2.5 THz [25].

* Corresponding author. Institute of Modern Optics, Nankai University, Tianjin, 300350, China.
** Corresponding author. Institute of Modern Optics, Nankai University, Tianjin, 300350, China.
E-mail addresses: fanfei@nankai.edu.cn (F. Fan), sjchang@nankai.edu.cn (S.-J. Chang).

https://doi.org/10.1016/j.carbon.2019.06.084
0008-6223/

However, in order to the required high phase retardation (*e.g.*, $\pi/2$ or π phase retardation), the birefringence coefficient of the currently existing LCs determines that the required thickness of the THz LC cell should be several hundred micrometers, which is a key problem in current THz LC devices. Hsieh et al. have accomplished greater modulation of up to $\pi/2$ by using a lateral field to avoid affecting the transmittance of the THz signals, but this design suffered from a very slow response [26]. Lin et al. have proposed a self-polarizing phase shifter with sub-wavelength metallic gratings as both transparent electrodes in the range of 0.2–2 THz. However, the driving voltage is still high and these electrodes were polarization selective [27]. Most recently, highly transparent ITO nanowhisker electrodes have been utilized in THz phase shifters, the phase shift exceeding $\pi/2$ at 1.0 THz was achieved in a 517 μm thick cell [28]. Unfortunately, large cell gaps often lead to several disadvantages such as poor pre-alignment, high operating voltage, and slow response. These bottlenecks hinder the development of the THz LC devices.

The dual-frequency liquid crystals (DFLCs), which consists of a mixture of LCs with different anisotropy, exhibit positive ($\Delta\varepsilon>0$) or negative dielectric anisotropy ($\Delta\varepsilon<0$) depending on the alternating (*AC*) frequencies in an external *AC* electric field. Owing to its unique *AC* frequency dependent dielectric features, application of DFLC has been reported in various electro-optical and fast-switching devices [29–31]. Chen et al. demonstrated an electrically controllable THz metamaterial combined with DFLC cell, in which the resonance frequency can be continuously moved by changing the *AC* frequency of the external electric field [32]. Besides, Göbel et al. also realized a tunable THz filter based on the DFLC [33]. Yu et al. explored the *AC* frequency-dependent anisotropic property of DFLC and its tuning rules in the THz regime, and a tunable quarter-wave plate above 0.68 THz has been obtained in a 600 μm thick DFLC cell [34]. In short, the DFLCs will be of great significance for active THz phase and polarization control devices, which breaks through the traditional working mode of rotation of LC molecules depending on the voltage. Under a certain voltage, the orientation of LC molecules can be controlled by the *AC* frequencies, this unique working mode not only ensures fast response, but also no longer relies on initial anchoring. However, the birefringence and tuning range of the existing DFLC in the THz regime are still small, and some improvements are urgently needed.

Carbon nanotube (CNT), a functional nanomaterial that possesses extremely anisotropic electric, magnetic, and optical properties, has drawn much consideration in the THz regime [35–37]. LCs are attractive hosts for the dispersion and manipulation of CNTs, and the nanotube properties are also attractive for influencing and tuning LC properties. Therefore, CNTs dispersed in LCs represents an interesting anisotropic composite system, which can not only enhance the orientation of LC molecules on CNT surface but also improve the mechanical, electrical and electro-optical properties of LCs, such as the large nonlinear optical effect [38,39], the enhancement of electro-optical effects [40,41] and dielectric and electrical properties [42,43]. However, the electro-optical and dielectric anisotropic properties of the composite of CNTs dispersed in DFLCs in the THz regime have been reported rarely.

In this paper, we experimentally investigated the dielectric anisotropic enhancement characteristics of the CNT-LC in the THz regime. The tuning phase range of the CNT-LC (1.5 wt%) at 0.793 THz is 0.5π, which is 0.12π higher than the pure DFLC, thereby improving the working performance effectively. Furthermore, the CNT-LC (1.5 wt%) can work as a tunable quarter-wave plate at 0.925 THz when $f_{AC} = 100$ kHz, which cannot be achieved in pure DFLC under the same conditions. We have experimentally and theoretically demonstrated that this dielectric anisotropic enhancement at high *AC* frequencies is due to the surface interaction of the CNTs inducing parallel orientations of the surrounding positive LC molecules. We believe that the improvement of the dielectric anisotropic by dispersing CNTs into DFLCs can provide an alternative approach for high-performance THz liquid crystal devices.

2. Materials and methods

CNTs used in our work are multi-wall carbon nanotubes with the diameter of 10–20 nm and the length of 5–15 μm, which were provided by Tokyo Chemical Industry (TCI) (CAS: 308068-56-6, product code: C2150). The DFLC, a mixture of LCs, was obtained from Jiangsu Hecheng Technology Co., Ltd. (DP002-016, HCCH, China). It exhibits a positive dielectric anisotropy ($\Delta\varepsilon > 0$) when the *AC* frequency is below f_c (crossover frequency) while turns to a negative one ($\Delta\varepsilon < 0$) at $f_{AC} > f_c$. The dielectric constants of this DFLC are +9.8 or −2.2 when $f_c = 1$ kHz or 100 kHz at 25 °C, respectively. CNT is mixed with DFLC to form CNT-LCs, and the CNT-LCs with different concentrations from 0.75 wt% to 3 wt% are obtained. The mixture was ultrasonicated for 4–6 h to reach dispersion of CNTs. The CNT-LCs are added to fill a 0.5 mm-thick LC cell, which is fabricated by five parallel copper wires sandwiched within two 600 μm-thick fused silica substrates. The copper wires serve alternatively as positive and negative electrodes. The 4 mm gap between adjacent copper wires ensures the electric field intensity is uniform and that the electrodes do not affect the transmission of THz waves, as shown in Fig. 1c. A square wave voltage (1–100 kHz, 0–100 V) is applied on the electrodes, and its *AC* frequency and intensity are controlled by the signal generator and voltage amplifier. The *AC* voltage is maintained as 100 V in our experiment, and the corresponding field intensity is 25 kV/m. It is worth mentioning here that the LC molecules are randomly distributed without any alignment preprocessing in the absence of an applied electric field.

In addition, Fig. 1a shows the images of the CNT-LCs with a CNT concentration of 1.5 wt% using a 100 × optical microscope when applying an *AC* electric field of 0 kV/m, 25 kV/m ($f_{AC} = 1$ kHz) and 25 kV/m ($f_{AC} = 100$ kHz). The CNTs are randomly entangled into aggregates without an *AC* electric field applied owing to the strong van der Waals forces. After applying an *AC* electric field, the CNT aggregates gradually form CNT chains arranged along the direction of the external electric field at low *AC* frequencies, and these CNT chains are unwound at high *AC* frequencies. The key reason is that the existence of the surface interaction forces between the CNTs and the LC molecules, so that the arrangement of CNT is affected by the arrangement of LC molecules, which directly depends on different *AC* frequencies. The detailed interaction mechanism will be introduced in Section 3.4. Fig. 1b shows the terahertz time-domain polarization spectroscopy (THz-TDPS) system. The detail of this system and its data processing method can be found in Supplementary Information.

3. Results and discussions

3.1. Tuning range of THz phase in DFLC enhanced by CNTs

The THz-TDS spectra of the four samples are measured by the THz-TDPS system: pure DFLC without any CNTs labeled as LC (0 wt %), three DFLCs with different CNTs concentrations labeled as CNT-LC (0.75 wt%, 1.5 wt%, 3 wt%). As shown in Fig. 1b, THz wave was normally incident into the structure along the *z* axis with its polarization direction along the *y* axis, and the external electric field is along the *x* axis defined as $\phi = 0°$. The THz polarizer behind the samples is fixed at 0° in this section to detect the *y*-LP components. Fig. 1d shows the normalized time-domain signals of the THz pulse

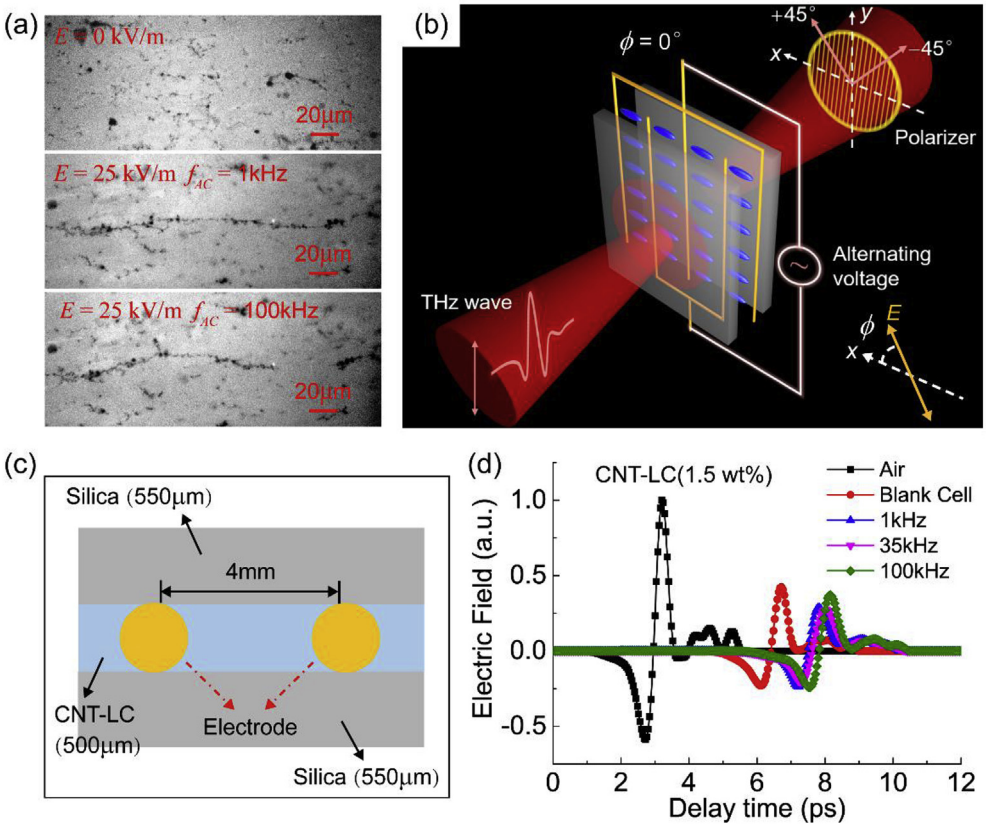

Fig. 1. (a) Optical microscopy photos of the CNT-LC in the absence or presence of an external electric field with different *AC* frequencies. (b) Experimental setup for phase and polarization measurement of the samples. The THz polarizer can be rotated from −45° to +45°. (c) Normalized THz time-domain signals of air, blank cell, CNT-LC (1.5 wt%) when f_{AC} = 1 kHz, 35 kHz, and 100 kHz. (d) The cross-section and geometric parameters of CNT-LC cell. (A colour version of this figure can be viewed online.)

in the air, in the blank cell, in CNT-LC (1.5 wt%) with the increase of the *AC* frequency from 1 kHz to 100 kHz.

When the f_{AC} increases from 1 kHz to 100 kHz, the time-domain signal delays of the four samples shown in Fig. 1d and Fig. S4 are increased, meaning that the refractive indices of the samples increase correspondingly, as shown in Fig. 2. The tunable range of refractive indices $dn = n_y\,(100\ \text{kHz}) - n_y\,(1\ \text{kHz})$ of the four samples at 1.0 THz were obtained, for example, $dn = 0.199$ for the CNT-LC (1.5 wt%), which is larger than $dn = 0.149$ for LC (0 wt%), so the tunable range of refractive index is significantly improved after doping CNTs into DFLC.

Fig. 3a further compares the relationship between the refractive index of *y*-LP components and the f_{AC} for the four samples at a certain THz frequency of 1.0 THz. As can be clearly seen, the tuning range of refractive index can be enhanced by dispersing CNTs into the DFLC and a critical concentration of CNT is 1.5 wt%. Similarly, the tuning range of phase varying with the *AC* frequency can be calculated by $d\delta = \delta_y\,(100\ \text{kHz}) - \delta_y\,(1\ \text{kHz})$, as shown in Fig. 3b, for example, $d\delta = 0.5\pi$ at 0.793 THz or $d\delta = 1.0\pi$ at 1.34 THz for the CNT-LC (1.5 wt%), while the tunable phase range for the LC (0 wt%) is 0.38π or 0.73π with the same LC layer thickness, much lower than the CNT-LC (1.5 wt%). Therefore, the tuning phase range is significantly increased at the same frequency point when CNTs are dispersed in the DFLC, which can be used as a tunable THz LC phase shifter.

3.2. THz dielectric anisotropy of DFLC

Next, we measured THz time-domain signals of ±45° LP components for the LC (0 wt%) and the CNT-LC (1.5 wt%) by rotating the angle of the THz polarizer in order to obtain the output polarization states of samples. The amplitude and phase spectra of the two samples can be obtained by using Fourier transform to the THz time-domain signals of ±45° LP components. And then we calculate the corresponding parameters according to eqns (6)–(8) of Supplementary Information so that we can obtain their output polarization ellipsis at a certain frequency. In this way, the orientation status of DFLC molecules at different *AC* frequencies can be further deduced, which confirms the unique dielectric anisotropy of DFLC.

In the first configuration of experimental geometry, we apply an *AC* electric field along the *x* axis ($\phi = 0°$), and the polarization direction of incident LP THz wave is along the *y* axis. As shown in Fig. 4a and Fig. S5, the time-domain signals are delayed backward when the f_{AC} increases from 1 kHz to 100 kHz, but the pulses of ±45° LP components are always coincident without any phase differences, suggesting that all the output waves in the whole THz frequency range are close to LP states as shown in the insets of Fig. 4a. Obviously, though the birefringence of DFLC has been changed by the *AC* frequencies, the polarization state of the output light does not change. The above results are obtained only when the polarization of the incident light is parallel or perpendicular to the optical axis of the uniaxial crystal, so this experiment proves that the main optical axis of DFLC always remains along the direction of the external electric field (here is *x* axis), not depending on the *AC* frequency.

In the second configuration, we rotate the external electric field as 45° respect to the *x* axis ($\phi = 45°$). In this case, the main optical axis of DFLC is 45° respect to the *x* axis, the polarization direction of incident LP wave (along the *y* axis) is also 45° respect to the main optical axis of DFLC. Meanwhile, the detected ±45° LP components

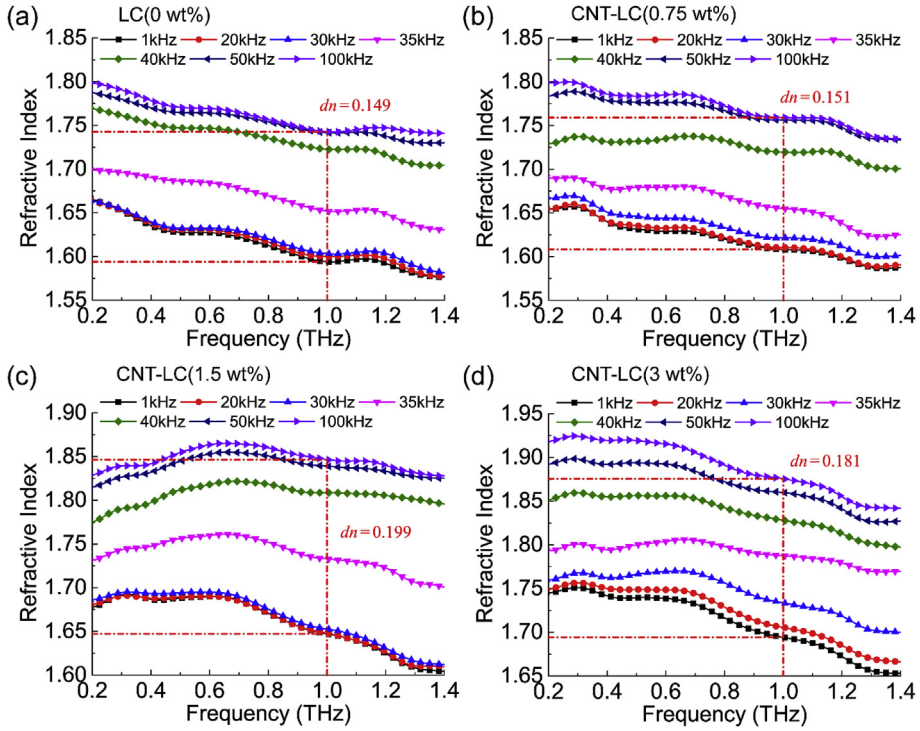

Fig. 2. Refractive index n_y of the four samples in the THz regime as the *AC* frequency increases from 1 kHz to 100 kHz. (a) LC (0 wt%); (b) CNT-LC (0.75 wt%); (c) CNT-LC (1.5 wt%); (d) CNT-LC (3 wt%). (A colour version of this figure can be viewed online.)

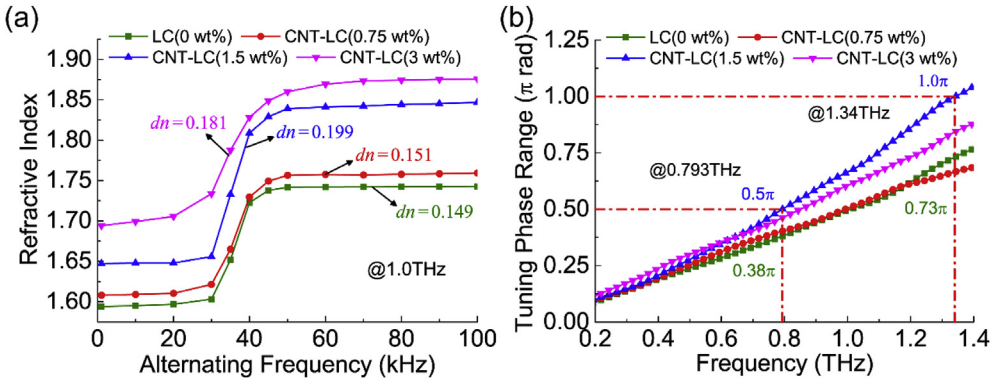

Fig. 3. Refractive index curves *v.s. AC* frequencies (a) and tuning phase range $d\delta$ between 1 kHz and 100 kHz (b) of the four samples: LC (0 wt%), CNT-LC (0.75 wt%), CNT-LC (1.5 wt%) and CNT-LC (3 wt%) in the THz regime. (A colour version of this figure can be viewed online.)

are parallel and perpendicular to the main optical axis of DFLC respectively, meaning that the obtained refractive indices here are the ordinary (n_o) and extraordinary refractive index (n_e) accordingly. Here, if the DFLC is anisotropy ($n_o \neq n_e$), the output polarization state should be converted. As shown in Fig. 4b, when $f_{AC} = 1$ kHz, there is a phase delay between the two time-domain signals of ±45° LP components, which means that the output wave is a CP light at 0.75 THz, because the phase difference between the ±45° LP components is just 0.5π at 0.75 THz. Then, the ±45° LP components gradually coincide when f_{AC} increases to the crossover frequency $f_c \approx 36$ kHz, so the output wave changes from a CP light to a LP light. Lastly, when the f_{AC} continues to increase to 100 kHz, the output wave gradually changes from a LP state to be an elliptically polarized (EP) light due to a phase delay occurring again between the two time-domain signals at 0.75 THz, and the rotation of this EP light is reversed to the first CP light. The similar processes can be observed in the experimental measurements of LC (0 wt%) by using THz-TDPS as shown in Fig. S6.

Furthermore, by using Fourier transform to the time domain signals of ±45° components, the refractive index spectra for the ordinary and extraordinary light of the LC (0 wt%) and the CNT-LC (1.5 wt%) at different *AC* frequencies are obtained in Fig. S7. For clarity, we select one THz frequency of 0.925 to draw the curves of n_o and n_e *v.s. AC* frequency in Fig. 5. It is clearly observed that the n_o is gradually increasing as the *AC* frequency increases, while the n_e is gradually decreasing, so the change of the refractive index is from $n_e > n_o$ to $n_e < n_o$. And then, we can obtain the refractive index ellipsoids of the LC (0 wt%) and the CNT-LC (1.5 wt%) at different *AC* frequencies, as shown by the insets of Fig. 5a and b. In brief, these results confirm that the tuning mechanism of the DFLCs depends

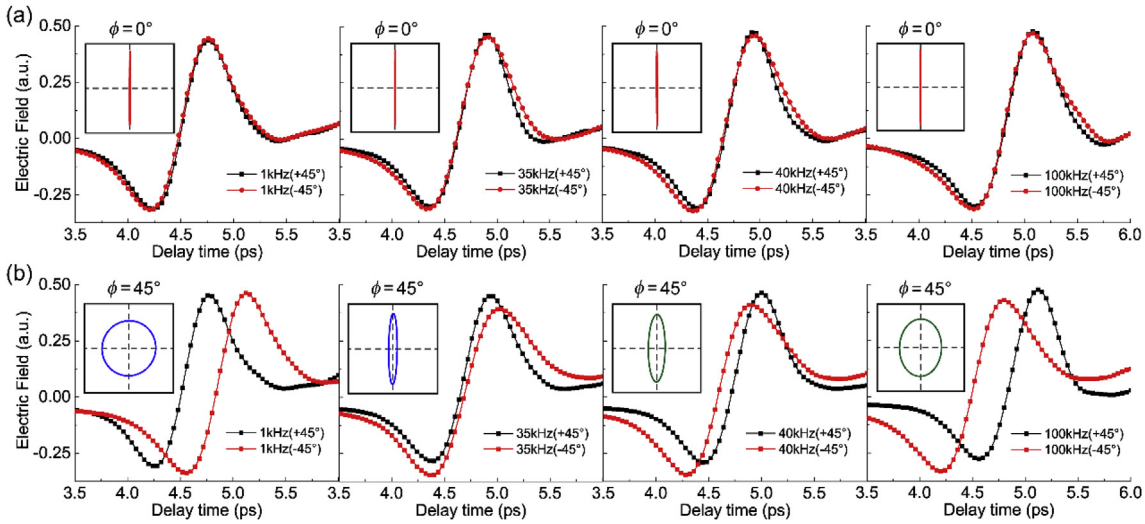

Fig. 4. Experimental THz time-domain signals of the CNT-LC (1.5 wt%) as the f_{AC} increases from 1 kHz to 100 kHz. (a) $\phi = 0°$; (b) $\phi = 45°$. The insets are their output polarization ellipsis at 0.75 THz. (A colour version of this figure can be viewed online.)

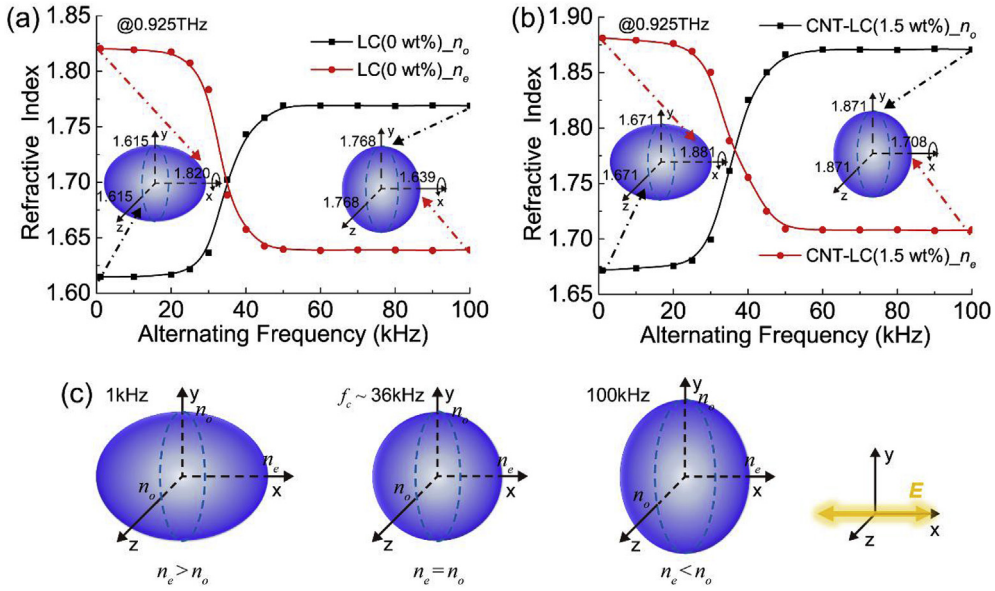

Fig. 5. The refractive index curves of the two samples as the f_{AC} increases: (a) LC (0 wt%); (b) CNT-LC (1.5 wt%). (c) Schematic diagrams of the equivalent refractive index ellipsoids of the CNT-LC (1.5 wt%) as the f_{AC} increases from 1 kHz to 100 kHz. (A colour version of this figure can be viewed online.)

on the change of its birefringence without changing its main optical axis: from positive dielectric anisotropy to dielectric isotropy, and then to negative dielectric anisotropy, which can be clearly described by the schematic diagrams of the refractive index ellipsoids shown in Fig. 5c. The detailed tuning mechanism of DFLC will be introduced in Section 3.4. We then calculated the birefringence $\Delta n = n_e - n_o$ as shown in Fig. S8, and the curves of Δn at 0.925 THz is shown in Fig. 6c. First, Δn of the LC (0 wt%) is closed to that of the CNT-LC (1.5 wt%) at low *AC* frequency of 1 kHz, for example at 0.925 THz, $\Delta n = 0.207$ for the LC (0 wt%) and 0.21 for the CNT-LC (1.5 wt%). Second, when the f_{AC} increases to 100 kHz, the birefringence of the CNT-LC (1.5 wt%) is −0.162 at 0.925 THz, which is larger than that of the LC (0 wt%) ($\Delta n = -0.131$). Therefore, the birefringence is gradually changed from positive to negative as the f_{AC} increases, and the birefringence at high *AC* frequencies is enhanced by dispersing CNTs into DFLCs.

3.3. DFLCs with or without CNTs as tunable THz wave plate

Similarly, the phase difference $\Delta\delta = \delta_e - \delta_o$ of the LC (0 wt%) and the CNT-LC (1.5 wt%) can be also calculated, where δ_e and δ_o are the extraordinary and ordinary phases, respectively. As shown in Fig. 6a and b, at a certain *AC* frequency, the phase difference increases linearly with THz frequencies; as the *AC* frequency increases, the phase difference at each THz frequency can be tuned from a positive value to 0, and then to a negative value. The whole tunable range of $\Delta\delta$ is just the regime between the black curve and green curves. If the phase difference $\Delta\delta$ can be tuned from $-\pi/2$ to $\pi/2$, this LC device can be used as a tunable quarter-wave plate to realize the active polarization conversion between (LP to LP) and (LP to CP). If the $\Delta\delta$ can be tuned from $-\pi$ to π, this LC device can be used as a tunable half-wave plate to realize the active polarization conversion from the LP to an arbitrary polarization state.

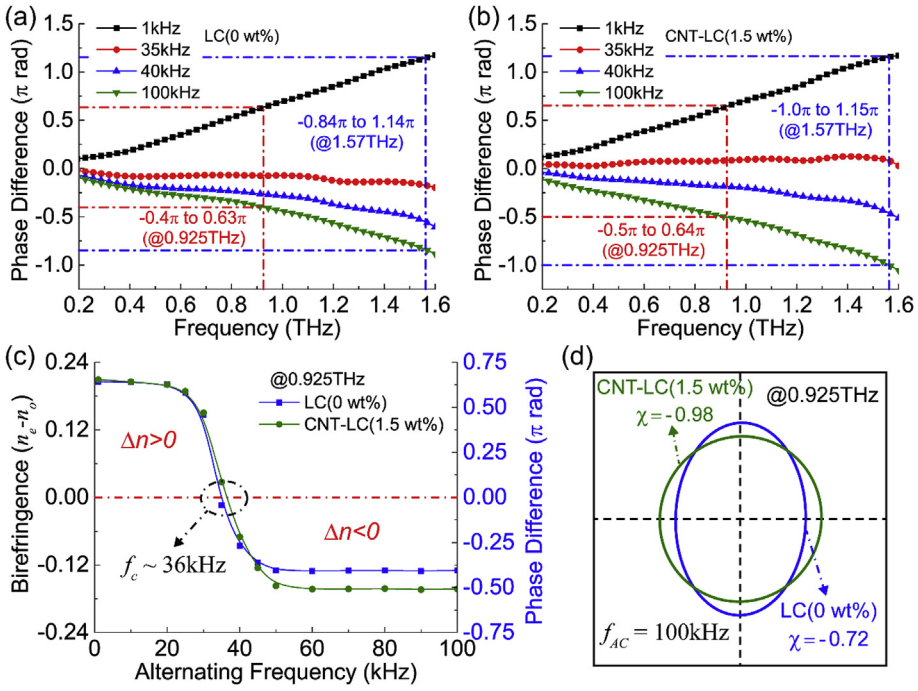

Fig. 6. The phase difference between the ordinary light and the extraordinary light of the two samples as the f_{AC} increases: (c) LC (0 wt%); (b) CNT-LC (1.5 wt%). (c) The birefringence and the phase difference between the ordinary light and the extraordinary light of the two samples as the f_{AC} increases. (d) The output polarization ellipsis of the two samples at 0.925 THz when f_{AC} = 100 kHz. (A colour version of this figure can be viewed online.)

Compared with LC (0 wt%) and the CNT-LC (1.5 wt%), the $\Delta\delta$ of the two samples are very closed at low *AC* frequencies, but the $\Delta\delta$ of the CNT-LC (1.5 wt%) increases more at high *AC* frequencies. For example, for the CNT-LC (1.5 wt%), $\Delta\delta = -0.5\pi$ at 0.925 THz and $\Delta\delta = -\pi$ at 1.57 THz, while the $\Delta\delta$ of the LC (0 wt%) is only -0.4π and -0.84π for the LC (0 wt%) at the same THz frequency. As a consequence, it can significantly enhance the birefringence and the phase difference by dispersing CNTs into LCs at high *AC* frequencies, and then the device's operating performance is improved accordingly. The output polarization ellipsis of the two samples at 0.925 THz when f_{AC} = 100 kHz are also obtained as shown in Fig. 6d, and we also calculate the ellipticity χ at this time, where $\chi = 0$ or ± 1 indicating a perfect LP or CP wave, respectively. Here, $\chi = -0.72$ for the LC (0 wt%) and $\chi = -0.98$ for the CNT-LC (1.5 wt%), which means that the CNT-LC (1.5 wt%) can work as a nearly perfect quarter-wave plate at 0.925 THz, while the LC (0 wt%) cannot realize this function.

3.4. Enhancement mechanism of dielectric anisotropy in CNT-LC

Next, we theoretically explain the above experimental phenomena with the orientation status of LC molecules and CNTs as shown in Fig. 7. Generally, A DFLC mixture is composed of two categories of materials [44]: positive and negative LC molecules, and the intrinsic dipole moments are located at the short axis of negative LC molecules and the long axis of positive LC molecules. The positive LC molecules exhibit positive dielectric anisotropy at low *AC* frequencies, but the dielectric anisotropy decreases as the *AC* frequency increases, which is the relaxation of dielectric permittivity along the long axis of positive LC molecules. At the same time, the negative LC molecules exhibit negative dielectric anisotropy and the dielectric anisotropy remains almost constant when the *AC* frequency is below the megahertz range. Thus, the reason for the unique dielectric anisotropy of the DFLC mixture is owing to the relaxation of dielectric permittivity of the positive LC molecules [45,46].

In the case of pure DFLCs, both the negative and positive LC molecules exist the molecular polarizing at low *AC* frequencies, thus the positive LC molecules are oriented along the direction of the external electric field, while the negative LC molecules are arranged perpendicular to the external electric field, and as a whole, the DFLC shows positive dielectric anisotropy when f_{AC} = 1 kHz, as shown in Fig. 7a. At a high *AC* frequency electric field up to 100 kHz, the positive LC molecules are no longer oriented along the external electric field, because the strong relaxation effect (*i.e.* its delayed response of high *AC* frequency electric field) eliminates the polarizing of positive LC molecules. While the negative LC molecules still maintain the same molecular polarizing direction along the external electric field. Consequently, the DFLC shows negative dielectric anisotropy as shown in Fig. 7c.

For the mixture of CNTs and DFLCs, there is a more significant surface interaction between the CNT cluster chains and the positive LC with long ellipsoidal chain molecule [47,48]. But notice that the polarizing effect of the external electric field on LC molecules is stronger than that of surface interaction between CNTs and LC molecules. As shown in the case at the low *AC* frequency of f_{AC} = 1 kHz in Fig. 7b, both the positive and negative LC molecules can respond to the *AC* electric field, so the result is similar to the case in Fig. 7a, and the CNTs are also oriented along the *AC* electric field because of surface interaction between CNTs and LC molecules. Additionally, the dielectric anisotropy of the CNT-LC is the same as that of the pure DFLC in this case, and this experimental result also indicates that even the CNTs with uniform alignment have little affection on the dielectric anisotropy of the CNT-LC under the low concentration. When f_{AC} = 100 kHz, the positive LC randomly arranged due to the polarizing relaxation, and the negative LC still maintain the same molecular polarizing direction, the surface interaction between negative LC molecules and CNTs is enough to make the CNT chains unwound, and induce CNTs to align along the orientation of the negative LC molecules. In turn, the CNTs also affect the orientation of the surrounding positive LC molecules

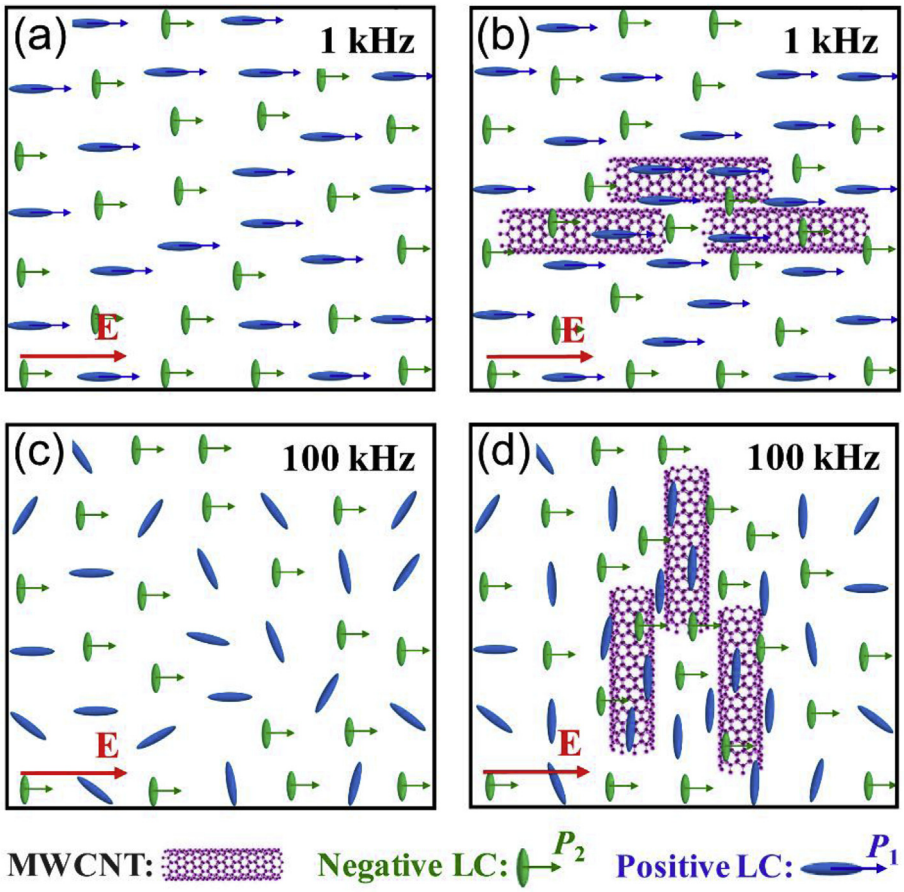

Fig. 7. Orientation states of DFLC molecules without or with different CNTs dispersing under different *AC* frequencies: (a) LC (0 wt%), $f_{AC} = 1$ kHz; (b) LC (0 wt%), $f_{AC} = 100$ kHz; (c) CNT-LC (1.5 wt%), $f_{AC} = 1$ kHz; (d) CNT-LC (1.5 wt%), $f_{AC} = 100$ kHz. (A colour version of this figure can be viewed online.)

arranged perpendicular to the direction of the external electric field, thus enhancing the negative dielectric anisotropy of the DFLC in this case, as shown in Fig. 7d. Overall, the reason for the enhancement of dielectric anisotropy of CNT-LC is that the surface interaction between CNTs and LC molecules makes a more uniform arrangement of the positive and negative LC molecules at high *AC* frequencies when the CNTs are added in the DFLC, rather than the negligible dielectric anisotropy of CNT itself.

It is worthwhile to note that the CNTs cannot follow the reorientation of the LC if the concentration of CNT is too large, because the orientation imposed by the aggregation cannot be easily overtaken, but if it is too small, the influence of CNTs on the properties of LCs can even be negligible. Therefore, the concentration is a critical parameter that is designed optimally as 1.5 wt% in this work.

4. Conclusions

In conclusion, we have experimentally demonstrated that the tuning mechanism of the DFLCs by using a THz-TDPS system, which depends on the change of its dielectric anisotropy without changing its main optical axis as the f_{AC} increases: from positive to negative dielectric anisotropy. This unique *AC* frequency-dependent anisotropic property originates from the different polarization relaxation response on the different *AC* frequency field for the positive and negative LC in DFLCs. Moreover, we also demonstrated that the reason for the negative dielectric anisotropy enhancement of the CNT-LCs at high *AC* frequencies is the surface interaction between the CNTs and the LC molecules. The results show that the tuning phase range of the CNT-LC (1.5 wt%) at 0.793 THz up to 0.5π, which can be used as a tunable THz phase shifter that is 0.12π higher than the pure DFLCs. Furthermore, an active polarization conversion from the LP to an arbitrary polarization state can be realized at 1.57 THz in the CNT-LC, while the pure DFLCs cannot be achieved within 1.6 THz frequency band. The dielectric anisotropy enhancement of the DFLCs with the doping of CNTs has significance for both THz LCs and CNTs materials, and potential applications for tunable THz phase shifter and wave plate.

Acknowledgements

This work was supported by the National Key Research and Development Program of China (2017YFA0701000), the National Natural Science Foundation of China (61831012, 61671491, 61505088), and the Young Elite Scientists Sponsorship Program by Tianjin (TJSQNTJ-2017-12).

Appendix A. Supplementary data

Supplementary data to this article can be found online at https://doi.org/10.1016/j.carbon.2019.06.084.

References

[1] S. Chen, F. Fan, Y.P. Miao, X.T. He, K.L. Zhang, S.J. Chang, Ultrasensitive terahertz modulation by silicon-grown MoS_2 nanosheets, Nanoscale 8 (8) (2016) 4713–4719.
[2] K.H. Jin, Y.G. Kim, S.H. Cho, J.C. Ye, D.S. Yee, High-speed terahertz reflection

three-dimensional imaging for nondestructive evaluation, Optic Express 20 (23) (2012) 25432–25440.
[3] L. Ho, M. Pepper, P. Taday, Terahertz spectroscopy: signatures and fingerprints, Nat. Photon. 2 (9) (2008) 541–543.
[4] S. Koenig, D. Lopez-Diaz, J. Antes, F. Boes, R. Henneberger, A. Leuther, et al., Wireless sub-THz communication system with high data rate, Nat. Photon. 7 (12) (2013) 977–981.
[5] Y. Chassagneux, R. Colombelli, W. Maineult, S. Barbieri, H.E. Beere, D.A. Ritchie, et al., Electrically pumped photonic-crystal terahertz lasers controlled by boundary conditions, Nature 457 (7226) (2009) 174–178.
[6] M. Shalaby, C.P. Hauri, Spectrally intense terahertz source based on triangular Selenium, Sci. Rep. 5 (2015) 8059.
[7] Y. Kawano, K. Ishibashi, An on-chip near-field terahertz probe and detector, Nat. Photon. 2 (10) (2008) 618–621.
[8] X. Cai, A.B. Sushkov, R.J. Suess, M.M. Jadidi, G.S. Jenkins, L.O. Nyakiti, et al., Sensitive room-temperature terahertz detection via the photothermoelectric effect in graphene, Nat. Nanotechnol. 9 (10) (2014) 814–819.
[9] R. Mendis, D.M. Mittleman, Comparison of the lowest-order transverse-electric (TE_1) and transverse-magnetic (TEM) modes of the parallel-plate waveguide for terahertz pulse applications, Optic Express 17 (17) (2009) 14839–14850.
[10] M. Sato, A. Yoshizawa, Electro-optical switching in a blue phase III exhibited by a chiral liquid crystal oligomer, Adv. Mater. 19 (23) (2007) 4145–4148.
[11] F. Fan, S. Chang, Y. Hou, Metallic photonic crystals for terahertz tunable filters, Sci. China Inf. Sci. 55 (1) (2012) 72–78.
[12] M. Shalaby, M. Peccianti, Y. Ozturk, R. Morandotti, A magnetic non-reciprocal isolator for broadband terahertz operation, Nat. Commun. 4 (2013) 1558.
[13] Y.X. Zhang, S. Qiao, S.X. Liang, Z.H. Wu, Z.Q. Yang, Z.H. Feng, et al., Gbps terahertz external modulator based on a composite metamaterial with a double-channel heterostructure, Nano Lett. 15 (5) (2015) 3501–3506.
[14] S.-T. Xu, F.-T. Hu, M. Chen, F. Fan, S.-J. Chang, Broadband terahertz polarization converter and asymmetric transmission based on coupled dielectric-metal grating, Ann. Phys. 529 (10) (2017) 1700151.
[15] Y.-Y. Ji, F. Fan, M. Chen, L. Yang, S.-J. Chang, Terahertz artificial birefringence and tunable phase shifter based on dielectric metasurface with compound lattice, Optic Express 25 (10) (2017) 11405–11413.
[16] H.T. Chen, W.J. Padilla, M.J. Cich, A.K. Azad, R.D. Averitt, A.J. Taylor, A metamaterial solid-state terahertz phase modulator, Nat. Photon. 3 (3) (2009) 148–151.
[17] T. Kan, A. Isozaki, N. Kanda, N. Nemoto, K. Konishi, H. Takahashi, et al., Enantiomeric switching of chiral metamaterial for terahertz polarization modulation employing vertically deformable MEMS spirals, Nat. Commun. 6 (2015) 8422.
[18] L. Liu, I.V. Shadrivov, D.A. Powell, M.R. Raihan, H.T. Hattori, M. Decker, et al., Temperature control of terahertz metamaterials with liquid crystals, IEEE Trans. Terah. Sci. & Tech. 3 (6) (2013) 827–831.
[19] L. Cattaneo, M. Savoini, I. Muševič, A. Kimel, T. Rasing, Ultrafast all-optical response of a nematic liquid crystal, Optic Express 23 (11) (2015) 14010–14017.
[20] Y. Du, H. Tian, X. Cui, H. Wang, Z.X. Zhou, Electrically tunable liquid crystal terahertz phase shifter driven by transparent polymer electrodes, J. Mater. Chem. C 4 (19) (2016) 4138–4142.
[21] C.J. Lin, Y.T. Li, C.F. Hsieh, R.P. Pan, C.L. Pan, Manipulating terahertz wave by a magnetically tunable liquid crystal phase grating, Optic Express 16 (5) (2008) 2995–3001.
[22] N. Vieweg, M.K. Shakfa, M. Koch, BL037: a nematic mixture with high terahertz birefringence, Optic Commun. 284 (7) (2011) 1887–1889.
[23] R.P. Pan, C.F. Hsieh, C.L. Pan, C.Y. Chen, Temperature-dependent optical constants and birefringence of nematic liquid crystal 5CB in the terahertz frequency range, J. Appl. Phys. 103 (9) (2008), 093523.
[24] L. Wang, X.W. Lin, X. Liang, J.B. Wu, W. Hu, Z.G. Zheng, et al., Large birefringence liquid crystal material in terahertz range, Opt. Mater. Express 2 (10) (2012) 1314–1319.
[25] M. Reuter, N. Vieweg, B.M. Fischer, M. Mikulicz, M. Koch, K. Garbat, et al., Highly birefringent, low-loss liquid crystals for terahertz applications, Apl. Mater. 1 (1) (2013), 012107.
[26] C.F. Hsieh, R.P. Pan, T.T. Tang, H.L. Chen, C.L. Pan, Voltage-controlled liquid-crystal terahertz phase shifter and quarter-wave plate, Opt. Lett. 31 (8) (2006) 1112–1114.
[27] X.W. Lin, J.B. Wu, W. Hu, Z.G. Zheng, Z.J. Wu, G. Zhu, et al., Self-polarizing terahertz liquid crystal phase shifter, AIP Adv. 1 (3) (2011), 032133.
[28] C.S. Yang, T.T. Tang, R.P. Pan, P. Yu, C.L. Pan, Liquid crystal terahertz phase shifters with functional indium-tin-oxide nanostructures for biasing and alignment, Appl. Phys. Lett. 104 (14) (2014) 141106.
[29] Y.C. Hsiao, C.Y. Wu, C.H. Chen, V.Y. Zyryanov, W. Lee, Electro-optical device based on photonic structure with a dual-frequency cholesteric liquid crystal, Opt. Lett. 36 (14) (2011) 2632–2634.
[30] Y.C. Hsiao, Z.H. Yang, D. Shen, W. Lee, Red, green, and blue reflections enabled in an electrically tunable helical superstructure, Adv. Opt. Mater. 6 (5) (2018) 1701128.
[31] M. Mrukiewicz, P. Perkowski, W. Piecek, R. Mazur, O. Chojnowska, K. Garbat, Two-step switching in dual-frequency nematic liquid crystal mixtures, J. Appl. Phys. 118 (17) (2015) 173104.
[32] C.C. Chen, W.F. Chiang, M.C. Tsai, S.A. Jiang, T.H. Chang, S.H. Wang, et al., Continuously tunable and fast-response terahertz metamaterials using in-plane-switching dual-frequency liquid crystal cells, Opt. Lett. 40 (9) (2015) 2021–2024.
[33] T. Göbel, P. Meissner, A. Gaebler, M. Koeberle, S. Mueller, R. Jakoby, Dual-frequency switching liquid crystal based tunable THz filter, in: Conference on Lasers and Electro-Optics/International Quantum Electronics Conference, OSA Technical Digest (CD), Optical Society of America, 2009 paper CThFF4.
[34] J.-P. Yu, S. Chen, F. Fan, J.-R. Cheng, S.-T. Xu, X.-H. Wang, et al., Tunable terahertz wave-plate based on dual-frequency liquid crystal controlled by alternating electric field, Optic Express 26 (2) (2018) 663–673.
[35] L. Ren, C.L. Pint, L.G. Booshehri, W.D. Rice, X. Wang, D.J. Hilton, et al., Carbon nanotube terahertz polarizer, Nano Lett. 9 (7) (2009) 2610–2613.
[36] R. Wang, L. Xie, S. Hameed, C. Wang, Y. Ying, Mechanisms and applications of carbon nanotubes in terahertz devices: a review, Carbon 132 (2018) 42–58.
[37] S.-T. Xu, S. Chen, L.-L. Mou, F. Fan, Z.-F. Liu, S.-J. Chang, Carbon nanotube attached subwavelength grating for broadband terahertz polarization conversion and dispersion control, Carbon 139 (2018) 801–807.
[38] W. Lee, H.-C. Chen, Experimental studies of diffraction by photoinduced permanent gratings in nanotube-doped liquid crystals, J. Phys. D Appl. Phys. 35 (18) (2002) 2260–2263.
[39] W. Lee, H.-Y. Chen, S.-L. Yeh, Surface-sustained permanent gratings in nematic liquid crystals doped with carbon nanotubes, Optic Express 10 (11) (2002) 482–487.
[40] F.M. Ion, C. Berezovski, R. Berezovski, G. Heimann, M. Moisescu, Effects of carbon nanotubes on the electro-optical properties of nematic liquid-crystal cells, Rom. Rep. Phys. 64 (4) (2012) 1011–1018.
[41] H.Y. Chen, W. Lee, Electro-optical characteristics of a twisted nematic liquid-crystal cell doped with carbon nanotubes in a DC electric field, Opt. Rev. 12 (3) (2005) 223–225.
[42] M.S.E. Peterson, G. Georgiev, T.J. Atherton, P. Cebe, Dielectric analysis of the interaction of nematic liquid crystals with carbon nanotubes, Liq. Cryst. 45 (3) (2018) 450–458.
[43] L.N. Lisetski, S.S. Minenko, V.V. Ponevchinsky, M.S. Soskin, A.I. Goncharuk, N.I. Lebovka, Microstructure and incubation processes in composite liquid crystalline material (5CB) filled with multi walled carbon nanotubes, Mater. Werkst. 42 (1) (2011) 5–14.
[44] M. Schadt, Liquid crystal materials and liquid crystal displays, Annu. Rev. Mater. Sci. 27 (1) (1997) 305–379.
[45] M. Schadt, Low-frequency dielectric relaxations in nematics and dual-frequency addressing of field effects, Mol. Cryst. Liq. Cryst. 89 (1–4) (1982) 77–92.
[46] H. Xianyu, S.T. Wu, C.L. Lin, Dual frequency liquid crystals: a review, Liq. Cryst. 36 (6–7) (2009) 717–726.
[47] S.P. Yadav, S. Singh, Carbon nanotube dispersion in nematic liquid crystals: an overview, Prog. Mater. Sci. 80 (2016) 38–76.
[48] W.W. Tie, S.S. Bhattacharyya, Y.G. Zhang, Z. Zheng, T.H. Lee, S.W. Lee, et al., Field-induced stretching and dynamic reorientation of functionalized multi-walled carbon nanotube aggregates in nematic liquid crystals, Carbon 96 (2016) 548–556.